The Canadian Journal of Mineralogy and Petrology

ISSN 2817-1713 Vol. 62, pp. 77-93 (2024)

DOI: 10.3749/2300028

# GROWTH AND STABILITY OF STRATIFORM CARROLLITE (CuCo<sub>2</sub>S<sub>4</sub>) IN THE TENKE-FUNGURUME ORE DISTRICT, CENTRAL AFRICAN COPPERBELT

# BJORN P. VON DER HEYDEN§

Department of Earth Sciences, Stellenbosch University, Private Bag XI, Matieland 7602, South Africa

# JEFFREY DICK

Key Laboratory of Metallogenic Prediction of Nonferrous Metals and Geological Environment Monitoring of Ministry of Education, School of Geosciences and Info-Physics, Central South University, Changsha, China

## RYAN C. ROSENFELS AND LUKE CARLTON

Department of Earth Sciences, Stellenbosch University, Private Bag X1, Matieland 7602, South Africa

# KRISTINA LILOVA, ALEXANDRA NAVROTSKY, AND TAMILARASAN SUBRAMANI

School of Molecular Sciences and Center for Materials of the Universe, Arizona State University, Tempe, Arizona 85287, USA

# BRIAN F. WOODFIELD AND ALEXIS GIBSON

Department of Chemistry and Biochemistry, Brigham Young University, Provo, Utah 84602, USA

#### Abstract

Carrollite (CuCo<sub>2</sub>S<sub>4</sub>) is the main ore mineral of the critical battery metal cobalt, yet, surprisingly, detailed characterization of its thermodynamic properties and of its trace element contents remain sparse in the scientific literature. To fill these knowledge gaps, we generated the first thermodynamic data set for carrollite using well-characterized samples obtained from the stratiform sulfide mineralization style at Fungurume 88 deposit in the Democratic Republic of Congo. Detailed mineralogical investigation of these same samples suggests that carrollite has limited ability to incorporate other 'sweetener' elements (except Cu and Ni) by substitution mechanisms. Modeling using CHNOSZ 2.0.0. software and an integrated Cu-Co-S-O thermodynamic data set provides insights into the stability of carrollite relative to other Co-bearing minerals under physicochemical conditions relevant to the Central African Copperbelt. Further exploration of these models indicates that dropping redox potential in the mineralizing system is insufficient to explain the mineralscale and deposit-scale zonation patterns commonly observed in Cu-Co deposits of the Central African Copperbelt. Instead, factors such as increasing pH, decreasing T, decreasing sulfur activity, or some combination of changing physicochemical parameters may need to be invoked to explain these zonation trends. At the Fungurume 88 deposit, the absence of linnaeite (Co<sub>3</sub>S<sub>4</sub>) suggests that ore precipitation occurred at temperatures cooler than 211 °C. From our pHlog/O<sub>2</sub> diagrams, and relative to higher temperatures, such a lower T regime is marked by a greater degree of offset between the modeled Cu and Co solubility contours, thus facilitating a more differentiated and zoned distribution of these two metals at the deposit scale. Our models are offered to the geoscience community as exceptionally useful tools for modeling and visualizing the Cu-Co-S-O systematics and may be applied to a variety of geological and geometallurgical questions in the Central African Copperbelt and other deposits elsewhere.

Keywords: carrollite, trace elements, thermodynamics, Fungurume, Copperbelt, linnaeite.

<sup>§</sup> Corresponding author contact: bvon@sun.ac.za; Tel.: +27 21 808 3122

## Introduction

The global demand for cobalt continues to rise, most notably because of its use as a strategic and technologyenabling metal in rechargeable lithium ion batteries, an essential component of the growing electric vehicle industry (Wilburn 2012, Nazarewicz 2016, Li & Lu 2020). Due to its ability to resist oxidation, it is also used in electroplating and in the production of alloys used in magnets, high-T steels, and jet engines (Barton et al. 2014). Almost two thirds of the cobalt needed to meet this societal demand derives from mining activity in the Central African Copper Belt (CACB). There it exists primarily as a byproduct of the mining of sediment-hosted stratiform copper deposits that are found in an 11 km-thick sedimentary sequence known as the Katanga Supergroup (e.g., François 1974, Cailteux et al. 2005). These deposits have received extensive scientific and industrial attention, with most studies seeking to characterize the mineralization on the deposit scale and to explain the genetic implications across the mineral province. Toward these ends, several studies have employed geochemical and thermochemical modeling approaches to obtain better insights (e.g., Muchez & Corbella 2012, 2016, Rosenfels 2021, Vasyukova & Williams-Jones 2022). However, a major hindrance to these modeling studies has been the absence of thermodynamic data for carrollite (CuCo<sub>2</sub>S<sub>4</sub>), the predominant ore mineral of cobalt in the CACB.

In a companion paper, Gibson et al. (2023) have presented the first thermodynamic data set for nearstoichiometric carrollite (Cu<sub>0.92</sub>Co<sub>2.07</sub>S<sub>4</sub>), determined from pristine stratiform carrollite grains obtained from the Fungurume 88 deposit (Rosenfels & von der Heyden 2022). This data set creates an exciting opportunity to further explore the genesis of Co and Cu mineralization in the CACB using the principles of equilibrium chemistry, element solubility, and mineral stability under variable environmental (physicochemical) conditions. To augment these thermodynamic modeling insights, we conducted a detailed study into the trace element distributions within these individual carrollite grains, since sulfide trace element signatures are increasingly being used as a proxy to help understand ore-forming processes (e.g., Babedi et al. 2022). Inasmuch as several studies have focused on carrollite mineral chemistry (Vaughan et al. 1971, Craig et al. 1979, Wagner & Cook 1999), surprisingly there is a dearth of reported trace element data for this economically important thiospinel mineral phase. Work carried out by Rosenfels & von der Heyden (2022) characterized the trace element makeup of carrollite from the Fungurume 88 deposit in the Democratic Republic of Congo (DRC), but these data are merely reported for the purpose of comparing its genesis to the stratigraphically overlying Fungurume 8 deposit. Also recently, Twigg *et al.* (2022) interpreted carrollite trace element patterns to infer multiple phases of Cu-Co mineralization in the Kakanda deposits of the CACB and to highlight possible issues if Re-Os geochronological approaches are applied to this mineral phase.

This study thus seeks to couple trace element chemistry results from laser ablation-inductively coupled plasma-mass spectrometry (LA-ICP-MS) spot and mapping approaches with new thermodynamic modeling insights derived from the software CHNOSZ (Dick 2019). These data are used to better explain the formation of stratiform carrollite grains from the Fungurume 88 deposit. These insights may be extrapolated to better understand the reasons for high Co endowment in the CACB, and to explain observed decoupling in Cu and Co spatial distributions (e.g., Annels & Simmonds 1984). The presented thermodynamic models (SI 1) and a tool for their visualization (SI 2) are expected to serve as useful research aides for workers focused on Cu-Co mineralization within the CACB and at other Cu-Co deposits elsewhere.1

# GEOLOGICAL SETTING

The Fungurume 88 deposit is located in the Tenke-Fungurume ore district in southeastern DRC and was recently studied in depth by Rosenfels & von der Heyden (2022). It is hosted in one of the numerous E-W trending tectonic windows of Neoproterozoic Roan group sediments or "escailles" that make up the ±400 km long Lufilian arc (Schuh et al. 2012; Fig. 1). The stratigraphic sequence exposed in the deposit comprises the Musonoi subgroup in the basal parts of the sequence, overlain by the Mines subgroup, and in turn overlain by minor Fungurume subgroup sediments. Copper-cobalt mineralization is predominantly hosted by and stratabound to the reduced units of the Mines subgroup (Cailteux et al. 2005, Hitzman et al. 2012). Currently, a prevalent metallogenic model used to explain this exceptional metal occurrence suggests a syn-sedimentary to early diagenetic phase of mineralization followed by a syn-orogenic phase, i.e., at least two mineralization episodes (El Desouky et al. 2009). There are two predominant mineralized horizons which define discrete orebodies within the Mines subgroup, although other stratigraphic units may be locally mineralized. The lower orebody is generally confined to the Roches Siliceuses Feuilletées (RSF) and Dolomies Stratifiées (D-Strat) units, and the upper orebody is found in the

<sup>&</sup>lt;sup>1</sup> Supplementary Data are available from the Depository of Unpublished Data on the MAC website (http://mineralogicalassociation.ca/), "Stratiform Carrollite, CM62, 23-00028".

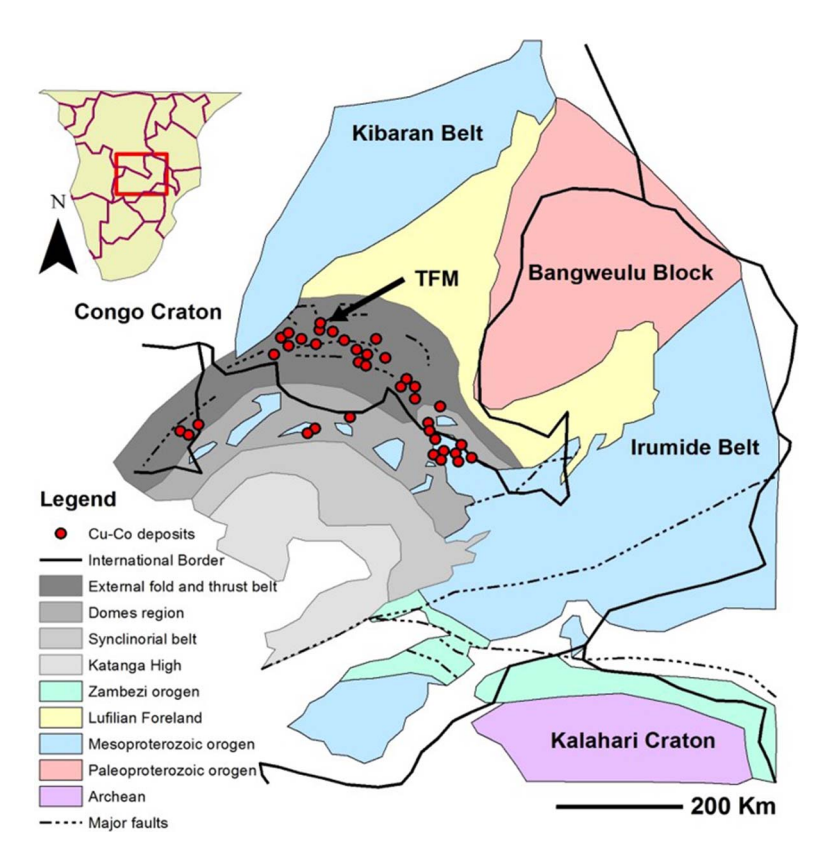


Fig. 1. Simplified regional geological map of the CACB located at the border between Zambia and the Democratic Republic of Congo (see inset). The various orogenic blocks, mobile belts, and parts of the Lufilian arc are detailed. Note the arrow indicating the location of the Tenke-Fungurume mining district (TFM). Modified after Kampunzu & Cailteux (1999) and El Desouky *et al.* (2009).

Shales Dolomitiques de Base (SDB) unit (Cailteux et al. 2005, Hitzman et al. 2012). The Fungurume 88 deposit underlies the Fungurume 8 deposit, which together have been interpreted to represent a thrust duplication of the sedimentary sequence (Rosenfels & von der Heyden 2022). The Fungurume 88 deposit is specifically unique since it hosts high-grade cobalt mineralization in a stratigraphic subunit that is usually regarded as being barren. This subunit, the SD-1b, consists of a dolomitic shale/ mudstone as opposed to a dolomitic sandstone/siltstone that has been recorded elsewhere in the Copperbelt (François 1974, Schuh et al. 2012). Rosenfels & von der Heyden (2022) attributed this lithological change to a facies variation reflecting paleo-environmental differences within the Katangan basin, and, as such, the different lithologies have differing capacities to induce precipitation of metal sulfides. These authors further highlight four different styles of hypogene mineralization comprising primary copper sulfides and carrollite viz., genetically related disseminated-, stratiform-, and jack-vein style (Schuh et al. 2012) mineralization, and paragenetically late cross-cutting vein mineralization. The quantitatively important stratiform-style carrollite is the one that was recently characterized for its thermodynamic properties (Gibson *et al.* 2023) and is thus the basis for this study.

### CARROLLITE GEOCHEMISTRY AND CRYSTALLOGRAPHY

Carrollite (CuCo<sub>2</sub>S<sub>4</sub>) (Fig. 2a) is an intermediate composition that resides between solid solution endmembers linnaeite (Co<sub>3</sub>S<sub>4</sub>) and the compound Cu<sub>3</sub>S<sub>4</sub>, which likely does not exist due to instability of the Cu (III) oxidation state (Vaughan *et al.* 1971, Wagner & Cook 1999). The other endmember minerals that constitute the thiospinel mineral group include polydymite (Ni<sub>3</sub>S<sub>4</sub>) and greigite (Fe<sub>3</sub>S<sub>4</sub>). Within the thiospinel mineral group, other intermediate solid solution compositions have been identified, including siegenite (CoNi<sub>2</sub>S<sub>4</sub>), fletcherite (CuNi<sub>2</sub>S<sub>4</sub>), and violarite (FeNi<sub>2</sub>S<sub>4</sub>). The diversity in this solid solution series is a result of the crystal chemistry-controlled cation substitutions taking place in both the tetrahedral and

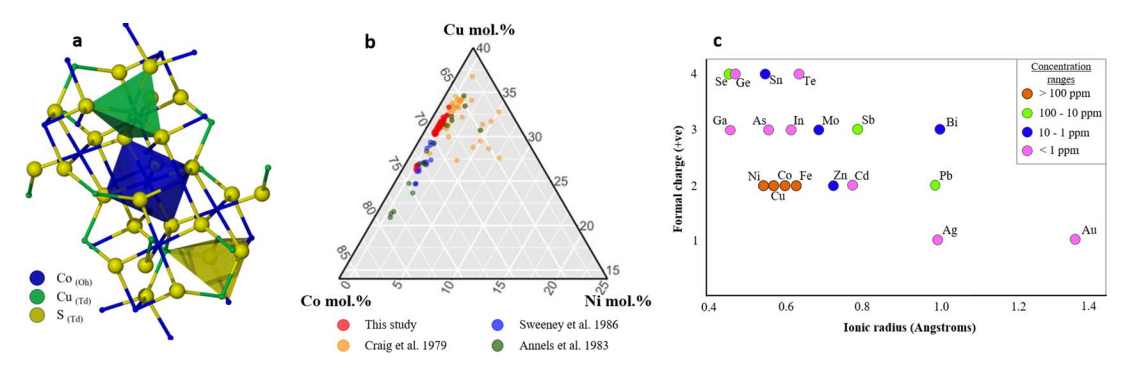


Fig. 2. (a) Mineral structure of carrollite highlighting low-spin Co<sup>3+</sup> in the octahedral site and Cu<sup>2+</sup> in the tetrahedral site, and with anionic sulfur also in tetrahedral coordination. (b) Cu–Co–Ni ternary diagram illustrating the distribution of these three dominant cations within the mineral structure of carrollite from the present study site (Rosenfels & von der Heyden 2022) and elsewhere. (c) Measured average concentrations of elements within carrollite from LA-ICP-MS spot analyses, distributed according to ionic size and charge properties. Note that only the dominant cationic valence state is shown for each element (figure adapted from Shannon 1976 and George *et al.* 2018).

octahedral sites of the spinel structure (Fig. 2; Vaughan et al. 1971). Much like other minerals of the spinel group, carrollite exhibits the cubic Fd3m crystallographic structure (Bosi et al. 2019). In this cubic close-packed arrangement, the unit cell contains eight AB<sub>2</sub>S<sub>4</sub> formula units with an approximate unit cell edge of 9.461Å (Vaughan et al. 1971). A common substitution into these sites is that of Ni and occasionally Fe, which can substitute for both Cu and Co (Craig et al. 1979, Annels & Simmonds 1984, Pattrick et al. 2008). Excess Co may also substitute into the structure through simple substitution of Co<sup>2+</sup> for Cu<sup>2+</sup> in the tetrahedral site (e.g., Gibson et al. 2023), although the metallic properties and delocalization of electrons negates formally attributing valence to the two crystallographic sites (Vaughan et al. 1971). Substitution of Ni into the carrollite crystal structure takes place by two separate mechanisms. Simple substitution involves replacement of Ni<sup>3+</sup> for Co<sup>3+</sup> at the octahedral sites or Ni<sup>2+</sup> for Cu<sup>2+</sup> at the tetrahedral sites (Wagner & Cook 1999). Coupled substitution mechanisms may also occur, involving the replacement reaction  $Ni^{3+} + Ni^{2+} \rightarrow$  $Cu^{2+} + Co^{3+}$  (Wagner & Cook 1999). The degree of Fe substitution into carrollite is more limited relative to Ni and becomes even more trivial as the amount of Ni increases (Wagner & Cook 1999).

Some geochemical studies conducted on thiospinel minerals include those on siegenite (Imai *et al.* 1973, Beckett-Brown *et al.* 2018), linnaeite (Ostwald 1978, Wagner & Cook 1999), violarite (Grguric 2002), and fletcherite (Craig & Carpenter 1977). Geochemical investigations on carrollite, on the other hand, are less common, and only its major element concentrations have been assessed. These include studies by Craig *et al.* (1979) and by Sweeney *et al.* (1986). The former, who investigated the phase relationships within the Cu–Co–S

system over a range of relatively high temperatures (400–900 °C), compiled a significant data set of cobalt rich-thiospinel compositions. These data were used to understand the chemical variability, metal ratios, and solid solutions within this group of minerals, though with somewhat limited applicability to the lower *T* conditions associated with the CACB. The latter study, which was centered around understanding the role of diagenesis in early sulfide mineralization in the Konkola basin of Zambia, reported the compositional variation of carrollites within its ore shale formation.

# Samples, Analytical Techniques, and Modeling Approaches

Optical petrography

Petrographic examination was conducted using a Zeiss Primotech® reflected light microscope to a maximum of 40× magnification. The petrographic examination considered 24 polished mounts of the stratiform carrollite and focused on discerning mineral identification, mineral textures, mineral parageneses, replacement phenomena, and relationships to host rock gangue phases (Fig. 3). All polished mounts were correctly orientated with respect to the drill core from which they were sampled (Rosenfels & von der Heyden 2022).

### Scanning electron microscopy (SEM)

SEM analysis was carried out on large, pristine carrollite and other primary sulfide grains from the four chosen samples in order to determine their major element geochemistry. This was achieved using a Zeiss EVO® MA15 scanning electron microscope with the

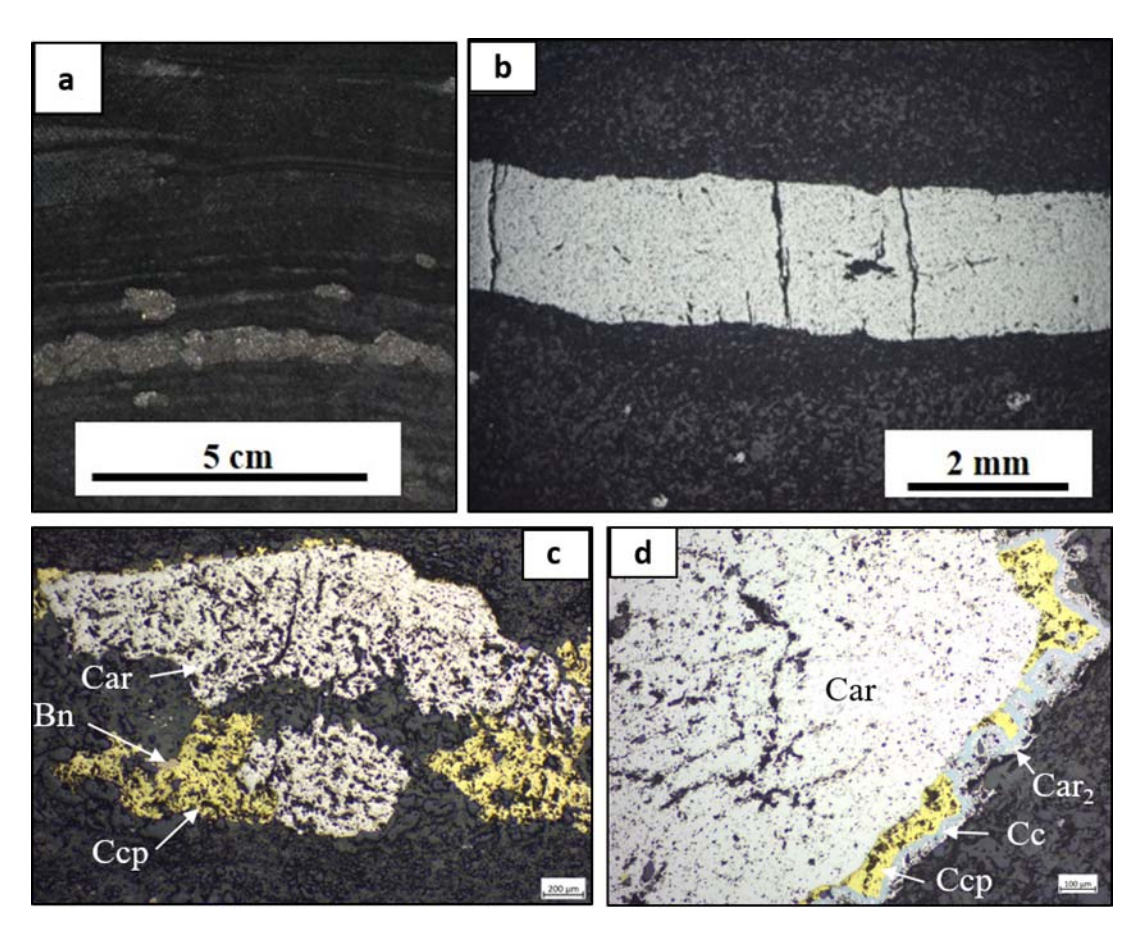


Fig. 3. Reflected light micrographs of stratiform carrollite mineralization taken at various scales. Magnified images (c, d) highlight early coarse-grained stratiform carrollite (Car) overgrown by later precipitation of chalcopyrite (Ccp), bornite (Bn), and chalcocite (Cc). In (d), a second generation of carrollite growth is observed (Car<sub>2</sub>).

combined energy dispersive spectrometry (EDS) of an Oxford Instruments® X-Max 20mm detector as well as a wavelength dispersive spectrometer (WDS). These analyses were conducted at the Central Analytical Facility (CAF), Stellenbosch University, RSA. Analyses were performed with a spot size of approximately 1 µm at an operating voltage of 20 kV and a beam current of 11 µA. The EDS and WDS data were collected simultaneously, and the detection limits are on the order of 0.1 wt.% and 0.01 wt.%, respectively. Thus, the major elements assessed include Cu, Co, and S (EDS), as well as Ni and Fe (WDS). Concentrations were determined relative to internationally accepted mineral standards (Astimex Scientific Limited, METM25-44 + FC Metal Standard Mount Serial No: 50-010 and Astimex Scientific Ltd. MINM25-53 Mineral mount Serial No: 03-040), and data reduction was performed using the Oxford INCA software based on the Phi-Rho-Z matrix correction procedure.

Laser ablation-inductively coupled plasma-mass spectroscopy (LA-ICP-MS)

Two LA-ICP-MS data sets were obtained for this analysis. The first was carried out on large, pristine carrollite grains, avoiding grain boundaries and replacement textures wherever possible. For this data set, a total of 62 spots were randomly ablated across the four selected samples. The second data set was obtained for the purpose of developing quantitative elemental maps, which are able to reveal concentration patterns within a single mineral grain as well as facilitate a rapid visualization of the partitioning trends among coexisting elements. For this data set, a set of parallel lines forming a grid across the mineral grain are predetermined, and in order to achieve adequate resolution the laser spot size was selected to match the distance between adjacent lines. Raster images were then produced using the integrated IDW function in ArcMap software. For both analyses, the trace elements measured include Ag, Au, Bi, Cd, Ga, Ge, In, Mo, Pb, Sb, Se, Sn, Te, and Zn, as well as major elements Cu, Co, Fe, Ni, and S. This was conducted using a 193 nm resolution excimer laser from Applied Spectra connected to an Agilent 7700 Q ICP-MS, also at the Central Analytical Facility (CAF), Stellenbosch University, RSA. After a spot size of 40 µm was determined, ablation took place within a helium (He)-filled sample cell in which the ablated material is then mixed with argon and a small amount of nitrogen before being transported to the ICP-MS. Here, the instrument ablation parameters (such as laser energy and frequency) are optimized while ablating on a synthetic sulfide standard (MASS-1) produced by the US Geological Survey. Data acquired from the SEM-EDS for S and from WDS analyses for Fe enabled the LA-ICP-MS <sup>34</sup>S and <sup>57</sup>Fe measurements to serve as internal standards. Data processing for both data sets was done using the LA-ICP-MS data reduction software package Iolite v.3.71 (Paton et al. 2011).

# Determining the thermodynamic properties of stratiform carrollite

The historical dearth of a robust thermodynamic data set for carrollite has been a noted hindrance in previous studies which sought to model Cu-Co ore-forming systems. To ameliorate this, a series of heat capacity measurements and oxide melt solution calorimetry analyses were conducted on the well-characterized stratiform carrollite samples from the Fungurume 88 deposit. Full details of these measurements are documented in Gibson et al. (2023), and only a brief synopsis is provided here. Approximately 15 mg of carrollite sample material was pressed into a pellet for measurement using a Quantum Design Physical Property Measurement System (PPMS) at Brigham Young University (Provo, UT, USA). Measurements were made in a zero magnetic field through the T range 1.9-300 K, following the methodologies set up for heat capacity measurements of insulating powders (Shi et al. 2010, 2011). A series of eight complementary oxide melt solution calorimetry measurements were conducted using a Setaram AlexSYS calorimeter at Arizona State University (Tempe, Arizona, USA). Measurements were collected at 1073 K using a sodium molybdate (3Na<sub>2</sub>O-4MoO<sub>3</sub>) melt as solvent and calibrated against the heat of combustion of 5 mg pellets of benzoic acid standard (C<sub>7</sub>H<sub>6</sub>O<sub>2</sub>, Parr Instruments). Further details of the application of this methodology to sulfide spinel minerals is provided elsewhere (e.g., Subramani et al. 2022, Gibson et al. 2023).

Modeling of thermodynamic properties using CHNOSZ

The log/O<sub>2</sub>-pH diagrams were made in CHNOSZ 2.0.0. (Dick 2019) using the scripts included as

supplementary material to this contribution (SI 1). To account for the formation of carrollite in a multi-metal system, the mosaic stacking feature of CHNOSZ was used (Dick 2021). Briefly, this starts with a basic mosaic diagram for minerals in the Cu-S-O system. In this first step, the mosaic accounts for the changing speciation of aqueous sulfur. The predominance fields of the Cu-bearing minerals calculated in the first step are themselves used to construct the mosaic in the second step. That is, the stable Cu-bearing minerals at each location on the diagram are used to write the formation reaction of the bimetallic mineral (carrollite). The affinity of this reaction is compared with the affinities for the reactions of the other Co-bearing minerals (without Cu), and the reaction with the highest affinity normalized by moles of Co indicates the stable mineral.

The default OBIGT thermodynamic database was used except for experimentally determined properties of carrollite and parameters for aqueous Co chloride complexes estimated from formation constants reported by Migdisov *et al.* (2011) (Table 1). The solubility calculations were performed using the solubility() function of CHNOSZ, which compares the solubilities for multiple minerals in a single-metal system; at each point on the diagram, the overall solubility is the minimum of those from all possible mineral dissolution reactions.

# Trace element speciation calculations using PHREEQC

Given that the carrollite mineral system is relatively understudied in terms of its trace element content and incorporation mechanisms, a preliminary PHREEQC modeling approach was used to test the solubility and speciation changes as a function of changes in the pH, pe, T, and total S content of a model precursor ore fluid. Previous work investigating metal adsorption onto sulfide mineral surfaces has highlighted the importance of pH as a primary control since this affects the metal complex speciation and degree of hydrolysis, in turn impacting the efficiency and extent of adsorption reactions between fluids and mineral surfaces (Jean & Bancroft 1986). Here, the composition of the mineralizing fluid is taken from previous modeling work conducted for the CACB (Muchez & Corbella 2012, 2016) in which the starting T is also set at 150 °C, and the trace element concentrations are pegged to the maximum values obtained for any single LA-ICP-MS spot analysis obtained in our detailed study of these carrollite grains. The llnl.dat database was used since this is the preferred database for higher T modeling in sulfide containing systems (Muchez & Corbella 2016). Each set of speciation calculations was conducted by keeping all major physicochemical parameters constant except the one being tested. For example, the impacts of pH were

TABLE 1. THERMODYNAMIC DATA FOR Co SULFIDE MINERALS AND Co CHLORIDE AQUEOUS COMPLEXES ADOPTED IN THIS STUDY

Name	Formula	$\Delta G_f^\circ$ J/mol	$\Delta H_{f}^{\circ}$ J/mol	S° J/K/mol	C <sub>p</sub> ∘ J/K/mol	√ cm³/mol	a J/K/mol	<i>b</i> J/K²/mol	c J K/mol	Note
carrollite	Cu <sub>0.92</sub> Co <sub>2.07</sub> S <sub>4</sub>	-331140	-344460	176.33	158.48	63.91	197.95	-0.0298	-2687000	В
							234.11	-0.1804	0	Q
cattierite	$CoS_2$	-147360	-153140	74.80	68.26	25.52	65.82	0.0303	-587000	ပ
linnaeite	Co <sub>3</sub> S <sub>4</sub>	-346350	-358990	175.94	162.63	63.12	153	0.0825	-1340000	ပ
Co-pentlandite	Co <sub>9</sub> S <sub>8</sub>	-816330	-850930	410.75	43.32	149.33	39.5	0.0271	-379000	ပ
CoCl+	C <sub>0</sub> Cl <sup>+</sup>	-190674	-228519	-50.69						р
CoCl <sub>2</sub>	CoCl <sub>2</sub>	-318845	-375729	62.33						ъ
CoCl <sub>3</sub> -	CoCl <sub>3</sub> -	-459477	-559857	93.33						ъ
CoCl <sub>4</sub> <sup>2-</sup>	CoCl <sub>4</sub> <sup>2-</sup>	-601033	-742683	131.79						р

Additional thermodynamic data not listed in this table were taken from Robie & Hemingway (1995) (all other Co minerals). Helgeson et al. (1978) (Cu minerals), and  $^a$   $^a$   $^d$   $G^a$ ,  $^a$ ,  $H^a$ ,  $^a$ , and  $^a$ , were taken from Gibson et al. (2023).  $^a$  was calculated by dividing the molar mass (308.694 g/mol) by the calculated density of carrollite Sverjensky *et al.* (1997) (Cu chloride aqueous complexes).  $\Delta G_f^p$ ,  $\Delta H_f^p$ ,  $S^p$ ,  $G_p^o$ , and  $V^p$  are standard molal thermodynamic properties at 25 °C and 1 bar, and a, b, and c are coefficients in the Maier-Kelley equation for heat capacity.

 $^b$  Transition occurs at 377 K with  $\Delta H_{tr}^\circ=$  162 J/mol. Heat capacity of the high-Tpolymorph was extrapolated above 392 K using a linear fit (Figure S3) 4.83 g/cm³) listed on https://www.mindat.org/min-911.html. Heat capacity coefficients were fit in this study to calorimetric data (Fig. S3)

<sup>c</sup> Pankratz et al. (1987) (as listed in Williams-Jones & Vasyukova 2022).

d Parameters obtained in this study by using the logB.to.OBIGT() function in CHNOSZ to fit the formation constants of complexes from spectroscopic data obtained and Shock & Helgeson (1988) for Co<sup>2+</sup> and Cl<sup>-</sup>, respectively. Using these parameters to extrapolate logK of formation reactions to 150 °C gives reasonable results at 200, 250, and 300 °C by Migdisov *et al.* (2011). Thermodynamic data for reference species in the formation reactions were taken from Sverjensky *et al.* (1997) SI 3, 4), but we caution against using these parameters to extrapolate far beyond the Trange of the experiments.

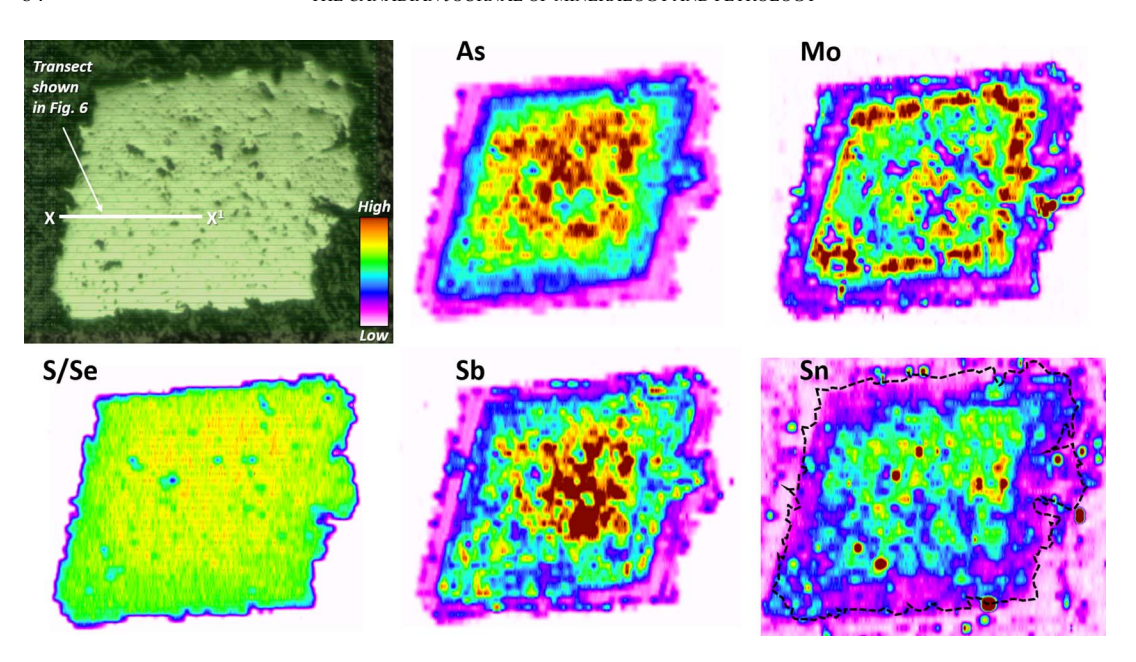


Fig. 4. A selection of LA-ICP-MS elemental maps showing zonation patterns observed in the trace element distributions within an individual stratiform carrollite grain. The position of the line indicates the transect data shown in Figure 6.

tested by allowing two fluids with different pH but constant pe, *T*, salinity, metal constant *etc*. to mix (at varying proportions) and equilibrate.

#### RESULTS

Stratiform carrollite major and trace element contents and distributions

The major element concentrations of the stratiform carrollite comprise between 18.44 and 19.45 wt.% Cu, 39.07 and 39.58 wt.% Co, and 40.70 and 41.48 wt.% S (Fig. 2b), which corresponds to a generalized stoichiometry of Cu<sub>0.92</sub>Co<sub>2.07</sub>S<sub>4</sub>. In agreement with the known solid solution series within the Co<sub>3</sub>S<sub>4</sub>-Cu<sub>3</sub>S<sub>4</sub>-Ni<sub>3</sub>S<sub>4</sub>-Fe<sub>3</sub>S<sub>4</sub> thiospinel system (e.g., Craig et al. 1979), Fe (606 ppm - 0.36 wt.%), and Ni (408 ppm - 0.15 wt.%)are quantitatively the most important trace element substituents identified and the only ones occurring at concentrations greater than 100 ppm (Fig. 2c). Elements that fall within the concentration bracket of 10-100 ppm include Pb, Sb, and Se, albeit that most of the data points cluster toward the low end of this range. The interquartile ranges for these three elements are, respectively, 2.83-11.31 ppm, 8.12-15.55 ppm, and 9.42-15.71 ppm (Fig. 2c). The elements that fall within the 1–10 ppm concentration range include Bi (8.44  $\pm$  4.98 ppm), Mo (6.34  $\pm$  4.90 ppm), and Zn (11.03  $\pm$  19.03 ppm). Elements incorporated at very low concentrations into the carrollite mineral structure (i.e., generally <1

ppm) include Ag, Au, Cd, Ga, Ge, In, Sn, and Te (Fig. 2c). Full data tables are available as open access data sets in Rosenfels & von der Heyden (2022) and Rosenfels (2021).

Figure 4 shows the elemental zonation present within an individual stratiform carrollite grain. Based on the resolution of the LA-ICP-MS mapping (40 µm spot size), the individual grains typically show a gradational zonation pattern in their trace element chemistry. Arsenic and Sb show a strong and consistent enrichment in the core of the individual grains; Ag, Cd, In, Sn, Zn also show preferential occurrences in the core of the grains, though concentrations are significantly lower and more sporadically developed. Molybdenum, Se, and, to a lesser extent, Te show preferential enrichments toward the rims of the individual grains (Fig. 4). We include a plot of the in situ S/Se ratio since this parameter has found extensive utility in studies of both hydrothermal and orthomagmatic sulfide mineralizing systems. The zonation map shows a consistent decrease in the S/Se ratio from core to grain boundary.

Thermodynamic stability of stratiform carrollite

In a companion paper (Gibson *et al.* 2023), these well-characterized natural stratiform carrollite grains were used to develop a first thermodynamic data set for carrollite. To augment the new carrollite data and to model the Co–Cu–S–O system in pH–logfO<sub>2</sub> space,

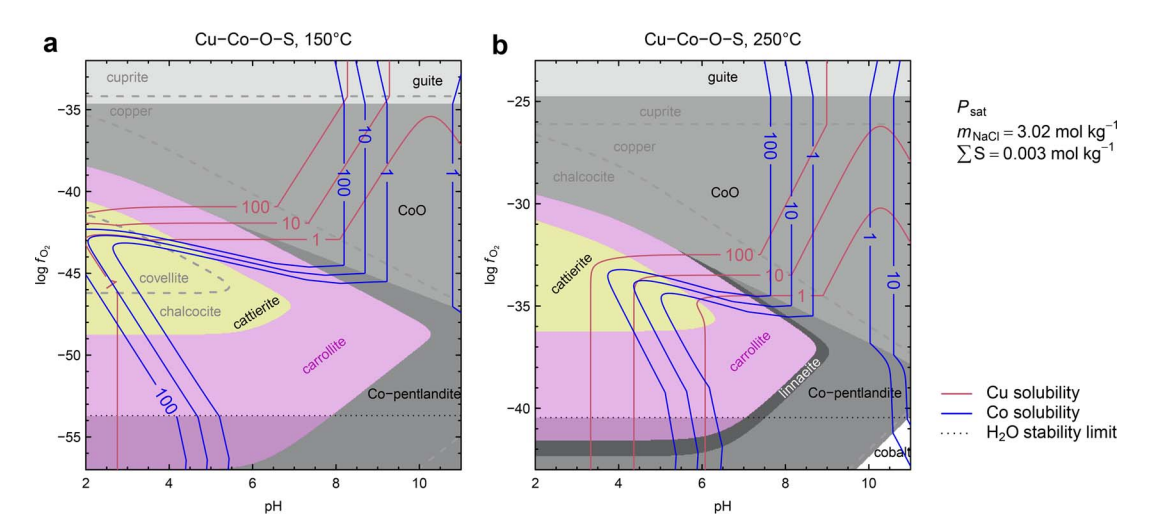


Fig. 5. log/O<sub>2</sub>-pH diagrams showing mineral stabilities at (a) 150 °C and (b) 250 °C in the Cu–S–O system (dashed gray lines) and the Co–Cu–S–O system (filled areas). The indicated molality of NaCl corresponds to 15% NaCl. Solubility contours (values are ppm) are overlaid for Cu in red and Co in blue. Solubility contours were calculated for single-metal systems and do not include carrollite; the inclusion of carrollite would have a slight effect on the solubility contours in the area where carrollite is stable (SI 5). Note that linneaite is calculated to not have a stability field at 150 °C (see also SI 6).

we collated the thermodynamic data sets for the other Co and Cu minerals (Table 1). The thermodynamic data for Cu oxides and sulfides in our study are sourced from Helgeson et al. (1978), but data for Co sulfides by necessity are from other sources, precluding the compilation of a verified internally consistent data set at this time. We adopted the data set for Co sulfides from Williams-Jones & Vasyukova (2022), who referenced the compilations of Robie & Hemingway (1995) for Co and Co oxides and Pankratz et al. (1987) for Co sulfides. Using the thermodynamic parameters compiled in Table 1, we predict that carrollite, but not linnaeite, is a stable mineral in the Co-Cu-S-O system at 150 °C and that the stability field of carrollite shrinks, whereas linneate is stabilized by increasing T to 250 °C (Fig. 5). Specifically, thermodynamic calculations indicate that linnaeite becomes stable at 211 °C and that carrollite is unstable above 438 °C (SI 5). This thermodynamic assessment agrees with the description of carrollite as a low-Tphase (e.g., Vaughan et al. 1971) and implies that under isothermal conditions at equilibrium compositionally controlled zonation between carrollite and linnaeite is only possible between 211 and 438 °C.

In combination with the revised thermodynamic data set described above, the modeling conditions tested for the CACB by Vasyukova & Williams-Jones (2022) serve as a useful platform from which to test the addition of carrollite data to the Cu–Co–S–O system (Fig. 5). Based on fluid inclusion data for fluids associated with CACB

stratiform style mineralization (Dewaele et al. 2006), the initial modeling conditions are set at 150 °C and 15 wt.% NaCl equivalents, with total sulfur set to 0.003 M (after Vasyukova & Williams-Jones 2022). The resulting plot generated using CHNOSZ software is shown in Figure 5a and is complemented by the model results generated when the T is increased to 250 °C (Fig. 5b). In the 150 °C calculation, the carrollite stability is sandwiched between the stability of fields for Co-pentlandite (which is generally more stable at higher pH conditions for the  $log f O_2$  range between -40 and -57) and cattierite (which is typically the stable phase at lower pH conditions for the  $\log O_2$  range between -40 and -49). Beyond the reducing water stability limit (which corresponds to unit fugacity of H<sub>2</sub>), carrollite+chalcocite is predicted to be stable at 150 °C, but this changes to Copentlandite+chalcocite as the dominant assemblage at 250 °C. The latter products were detected in experiments at 300 °C in pure H<sub>2</sub> (Bezverkhyy et al. 2003), lending support to the accuracy of the diagrams at reducing conditions.

Also shown in Figure 5 are the solubility contours for Cu and Co, which were separately calculated for minerals in the Cu–S–O and Co–S–O systems, respectively. Carrollite is not included in the calculation of solubility for either metal; however, it has a negligible effect on the positions of the solubility contours at the scale shown on this diagram (SI 6). The modeled solubility contours essentially replicate those reported in the 150 °C diagram presented by Vasyukova & Williams-Jones (2022), with

minor differences. In particular, at high pH, our contours suggest that species other than  ${\rm CuCl_2}^-$  and  ${\rm CoCl_4}^{2-}$  affect the solubility of Cu and Co, respectively.

## DISCUSSION

Empirical insights into the stratiform ore paragenesis

Published carrollite trace element data remain sparse in the literature (Rosenfels & von der Heyden 2022, Twigg et al. 2022) relative to the data available for other well-studied sulfides like pyrite (e.g., Babedi et al. 2022 and references therein). Even within the wellstudied pyrite mineral system, interpretations of trace element concentrations and distributions are hindered by a general lack in understanding of the kinetics, mechanisms, and efficiencies of trace element uptake by growing sulfide surfaces under evolving environmental conditions. These are impacted by hydrothermal fluid composition and associated trace element solubility, by surface chemistry reactions at variable reaction sites, and by crystallographic controls exerted by the sulfide mineral. Notwithstanding these concerns, the present section attempts to utilize trace element distributions to infer the evolution of the carrollite mineralizing system using a selection of proxies defined for other mineral systems.

Similarities in the geochemical behavior between S and Se are attributed to their positioning in adjacent rows on the periodic table, both as Group 16 elements. Whereas application of the S/Se ratio is well established for orthomagmatic Cu-Ni sulfide deposits (see review by Quefferus & Barnes 2015), its application to hydrothermal deposit classes is much more scant (Yamamoto 1976, Auclair et al. 1987, Layton-Matthews et al. 2005, 2008, Fitzpatrick 2008, Keith et al. 2018). The measured Se/S ratios in the stratiform carrollite samples studied record values of 0.12-2.16  $\times 10^4$ , which falls within the range of published data for pyrite, pyrrhotite, and chalcopyrite (Fitzpatrick 2008). Importantly, the LA-ICP-MS mapping shows a distinctive decrease in the S/Se ratio toward the grain boundaries (Fig. 4). The even distribution around all grain edges suggests that there is not a strong crystallographic control, in line with what has been shown previously by Chouinard et al. (2005) for Se incorporation into the pyrite mineral structure. We therefore suggest that the observed increase in Se concentration is related to changes in the fluid chemistry during stratiform carrollite growth under evolving diagenetic conditions. For oxidizing chloride-rich fluids, the Se/S ratio is predicted to increase with increasing pH or increasing fO2 (Yamamoto 1976). Huston et al. (1995) suggested that the Se/S ratio in pyrite relates principally to the  $\Sigma$ Se/ $\Sigma$ S in the initial solution, and both these authors and Keith *et al.* (2018) suggest that an increase in Se content correlates with a drop in *T*.

Other notable chemical zonation trends observed in the stratiform carrollite include those of As. Mo. Sb. and Sn. Several of these elements are used as proxies for T or redox characteristics of a diagenetic or mineralizing system. For example, Mo becomes increasingly enriched in marine sediments as the redox state becomes less oxic due to the particle reactive behavior of thiomolybdate (Bennett & Canfield 2020, and references therein). Although focused on a surface water body, Ullrich et al. (2013) showed that sulfur speciation has a strong ability to control both the concentration and speciation of ambient As and Sb. Figure 6b synthesizes the modeling results from the exploratory analyses using PHREEQC to test the trace element speciation changes in a model hydrothermal fluid that is relevant to the CACB (Muchez & Corbella 2012, 2016). The figure illustrates the impacts of changes in pH, both in terms of resultant changes to the relative amounts of the major valence states, and in terms of changes to the degree of hydrolysis between the two most dominant species (assumed to be the two species most likely to incorporate onto the carrollite surface). Changes to the pH can induce a significant impact on the speciation of the fluid complexes (Fig. 6b), however, the directionality of the modeled speciation responses did not consistently match the empirical trends measured for the carrollite grain. Similarly, drop in pe value and drop in T (both data sets not shown) could also not consistently replicate the observed results. Such an approach toward constraining the controls on mineralizing fluid evolution will benefit greatly from more robust characterizations of the speciation of trace elements in the carrollite mineral structure and from improved mechanistic insights into the processes responsible for trace element incorporation. A converse approach is that if the changing fluid physicochemical parameter is known, then the dominant mechanism of trace element incorporation may be narrowed down or predicted.

Thermodynamic modeling insights into the local and regional-scale metallogenic zonation trends in the CACB

From fluid inclusion studies, the physicochemistry of the fluids responsible for mineralizing the early diagenetic stage of Cu and Co in the CACB is loosely constrained to temperatures between 115 and 220 °C and salinities of between 11.3 and 20.9 wt.% NaCl equivalents (Dewaele *et al.* 2006, McGowan *et al.* 2006, Greyling 2009, El Desouky *et al.* 2009). There is a general acceptance that the fluid was relatively oxidizing (*e.g.*, Unrug 1988, Cailteux *et al.* 2005, El Desouky *et al.* 2010, Hitzman *et al.* 2010, Vasyukova

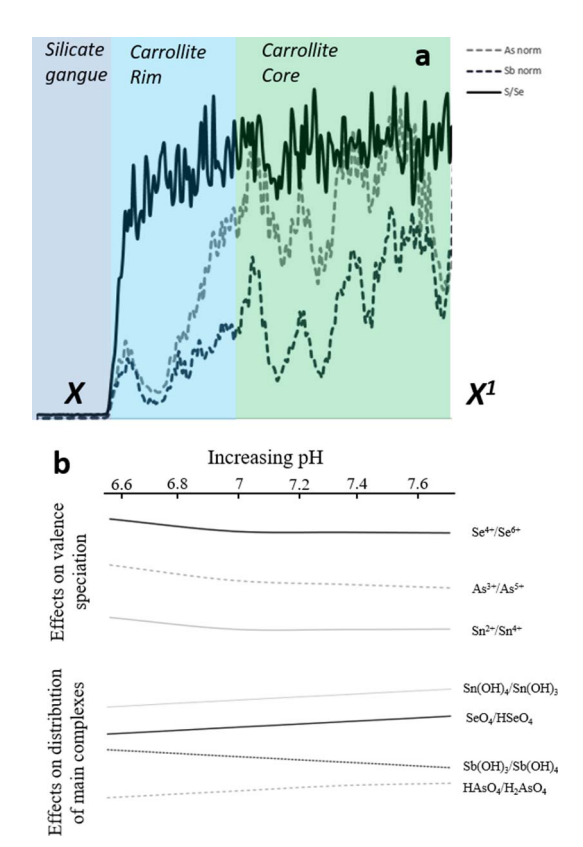


Fig. 6. (a) LA-ICP-MS transect X–X<sup>1</sup> (see Fig. 4a) showing a selection of the well-zoned elemental trends (As, Sb, and S/Se) between the core and rim of an individual carrollite grain. (b) PHREEQC modelling results showing the effects of increasing pH on the relative abundance of valence species in a model CACB ore fluid (Muchez & Corbella 2012, 2016). Similarly, the lower panel shows the effect of pH on the relative abundance in a model hydrothermal fluid of the two most dominant complexes associated with each zoned element.

& Williams-Jones 2022). Given the intimate associations between Co and Cu throughout the CACB, and given that efficient sulfide precipitation is achieved with rapid solubility drops through the 'transport window' (Jansson & Liu 2020), the positions of the solubility contours relative to the mineral stability fields in Figure 5 support this range of predicted ore fluid physicochemical conditions. The newly generated carrollite thermodynamic data set allows a first opportunity to explore the conditions under which this important Co phase may have mineralized. Although the preceding section alludes to some of the physicochemical changes that may have impacted trace element zonation, these results remain at present equivocal. Instead, we follow the approach of Vasyukova & Williams-Jones (2022),

in which regional-scale mineral zonation trends are used as a sanity check of the modeling interpretations of fluid evolution. These previously established trends suggest that Co has a strong tendency to enrich at the fringes of copper-dominant ore bodies both laterally and vertically within deposits of the Zambian Copperbelt (Annels & Simmonds 1984). Furthermore, these authors highlight that within the Co enriched zone, the minerals follow a pattern from carrollite through linnaeite and finally into Co-pentlandite with distance outward from the main Cu zone.

Figure 7 extends the standard pH-logfO<sub>2</sub> diagram into three-dimensional space (e.g., Huang 2016) to additionally explore the impacts of T and sulfur concentration on the stability of carrollite relative to other Cu and Co minerals. These 3D models are available as part of the supplementary material (SI 2) for other workers to explore as part of their interrogation of the CACB or other Co-Cu deposits globally. For these model-guided theoretical explorations, the fluid starting conditions are taken as being above the 100 ppm Co solubility contour (i.e., upper limit of the Co 'transport window'), but within the carrollite stability field to ensure that this is the first mineral to precipitate. The offset between the Cu-solubility contours and the Co solubility contours ensures that at this starting composition, much of the Cu should already have precipitated out. In fact, this offset likely represents the first order control on the observed zonation trends in the CACB. That is, under environmental conditions in which the Co- and Cu-solubility contours are further offset with respect to one another (e.g., at 150 °C; Fig. 5a), the zonation effects are likely to be more pronounced than when these contour sets are closely spaced (e.g., at 250 °C; Fig. 5b).

The most prevalent theory for an ore precipitation mechanism is reduction of the oxidizing ore fluid by either interaction with a reducing organic carbon-rich host lithology or by bacterially mediated processes (e.g., Unrug 1988, Cailteux et al. 2005, El Desouky et al. 2010, Hitzman et al. 2010, Vasyukova & Williams-Jones 2022). In the CACB, the redox front is typically marked by finer-grained organic rich sediments of the Mines Subgroup (Unrug 1988, Hitzman et al. 2010). Given the sub-horizontal orientation of the Co solubility contours (Fig. 5), a decrease in the log/O<sub>2</sub> parameter is indeed an efficient mechanism for precipitating carrollite. With progressive decreases in logfO2, however, the modeled paragenetic sequence suggests that carrollite precipitation will be followed by precipitation of cattierite, and would thus not explain the zonal trends observed by Annels & Simmonds (1984), or the textural observations of Cailteux et al. (2005) in which linnaeite-group minerals (including carrollite) postdate the precipitation of cattierite. Given its importance in controlling trace element uptake by sulfide surfaces (discussed in a previous section; Jean & Bancroft

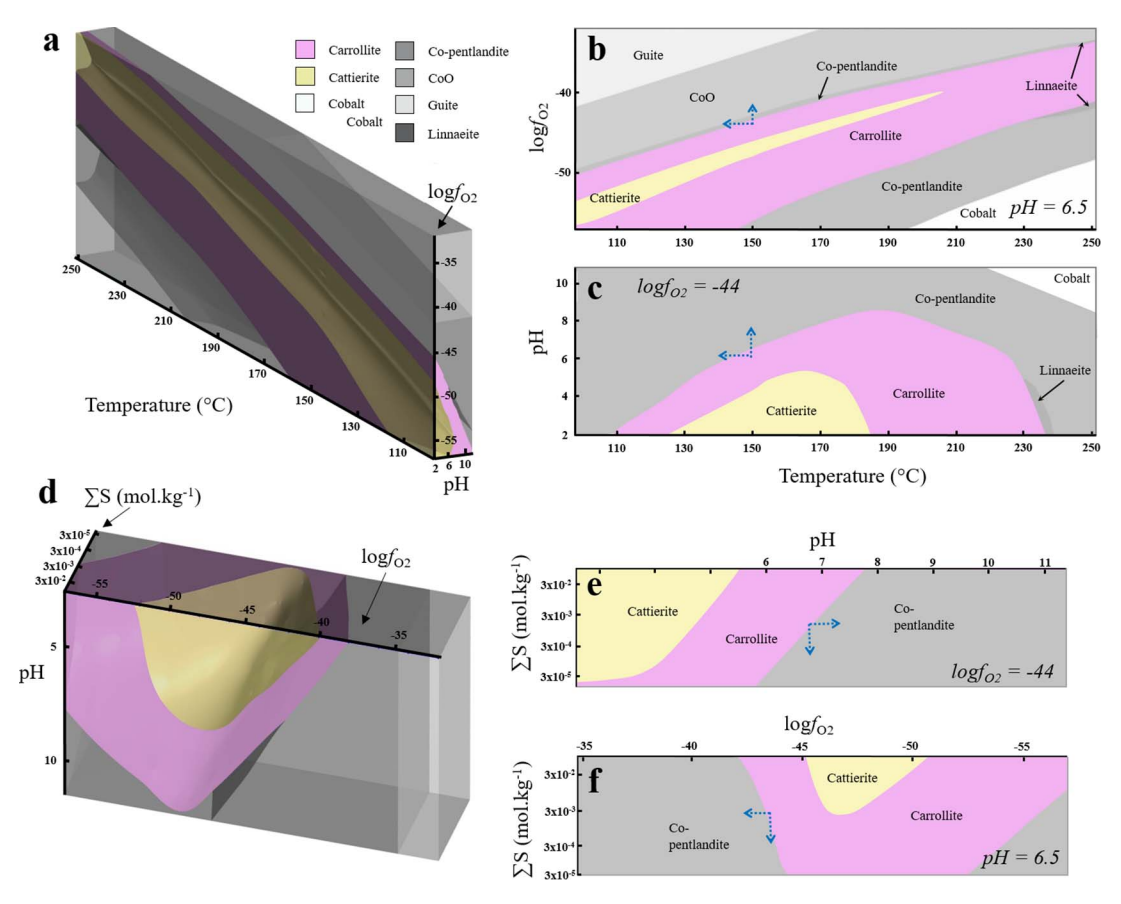


Fig. 7. (a–c) Semi-quantitative 3D model showing the stability of carrollite and other Co minerals in pH–logf<sub>O2</sub>–T modeling space. (d–e) Three-dimensional visualization of mineral stability fields in pH–logf<sub>O2</sub>–[total S] space. In each subfigure (b, c, d, e), the blue stippled arrows reflect the directionality of the change in parameters that would result in a zonation trend grading from carrollite → (linnaeite) → Co-pentlandite. Additional modeling and visualization tools are available in SI 1 and SI 2. For better resolution of the color scheme, please consult the interactive Leapfrog visualization software in SI 2 in which color schemes can be modified.

1986), the influence of pH is the second parameter to be tested using the thermodynamic models presented in Figure 5. In contrast to a drop in  $\log f_{\rm O2}$ , the modeled increases in the pH of the system suggest a result that matches the observed paragenetic sequence. For example, under a higher T regime where linnaeite is stable (e.g., 250 °C; Fig. 5b), the paragenetic sequence is modeled to follow the order carrollite  $\rightarrow$  linnaeite  $\rightarrow$  Co-pentlandite as pH increases between 7 and 8 at  $\log f_{\rm O2} = -35$ . Although this paragenetic sequence agrees with previously reported local zonation trends (Annels & Simmonds 1984), the sub-horizontal Co solubility contours over this pH interval suggest that this is an inefficient mechanism for Co sulfide precipitation.

In most geological environments, except those in which fluid mixing mechanisms are invoked, T

differentials within rock masses are too low to provide an efficient mechanism for concentrated ore precipitation (e.g., Robb 2020). At least one study has suggested fluid mixing as a viable mechanism for ore precipitation (Sutton & Maynard 2005), and this mechanism thus warrants testing using the new thermodynamic model (Figs. 5, 7a-c). Decreasing T has the effect of shifting the modeled mineral stability fields to lower logfO<sub>2</sub> values, while also increasing the offset between the Co- and Cu-solubility contours (Fig. 5a, b). Importantly, T also has a strong control on the stability of linnaeite (SI 5) and our data set suggests that deposits in which both linnaeite and carrollite are stable (Cailteux et al. 2005 and references therein) must have formed in the T range 211–438 °C. These temperatures lie toward the upper end of the

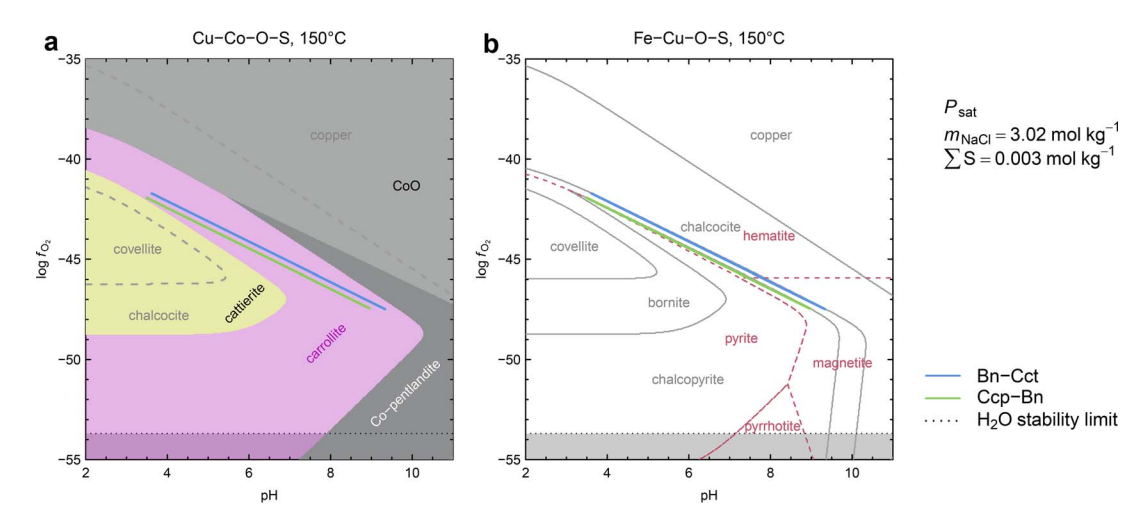


Fig. 8. Comparison of relative stabilities of Fe-Cu minerals with the carrollite stability field shows that reactions involving all these minerals may occur at relatively high pH. (a) Selected segments of bornite-chalcocite (blue) and bornite-chalcopyrite (green) reactions overlaid on the diagram for Cu-Co-O-S minerals. (b) Fe-Cu-O-S system with the segments in (a) highlighted.

range of temperatures predicted for the early diagenetic phase of ore formation (Dewaele *et al.* 2006, McGowan *et al.* 2006, Greyling 2009, El Desouky *et al.* 2009). The modeled effects of decreasing T suggest that at constant pH and  $\log fO_2$ , T differentials of as little as 5 °C may be sufficient to account for the observed regional zonation trends (Fig. 7a–c). However, a decrease in T has the effect of moving the solubility contours to lower  $\log fO_2$  values, implying that the solubility of Co increases with decreasing T, whereas Cu remains relatively insoluble.

The final parameter tested in this modeling work is a decrease in the total S concentration (Fig. 7d-f), as hypothesized by the observed trends in decreasing S/Se ratio within individual stratiform carrollite grains (Fig. 4). Decreases in the sulfur activity in the system have the effect of shrinking the size of the various mineral stability fields (Fig. 7d-f). Thus, for constant pH and  $log fO_2$ , a decrease is the S concentration by a factor of 10 will similarly manifest as an evolving ore fluid, which sequentially precipitates carrollite  $\rightarrow \pm$  linnaeite (at temperatures >211 °C)  $\rightarrow$  Co-pentlandite, in agreement with the trends reported in Annels & Simmonds (1984). Similar to the effects of decreasing T, a drop in S activity under oxidizing near-neutral conditions leads to an increase in the Co solubility, whereas Cu remains below its 'transport window'. A mechanism such as this may explain the later overgrowths of Cu minerals around carrollite (Fig. 3c, d) observed in this study and elsewhere. Indeed, preliminary modeling of the combined Cu-Co-Fe-O-S-Cl chemical system (Fig. 8) suggests that a relative vertical trajectory through the mineral stability fields will result in the Cu mineral assemblage evolving from chalcopyrite ( $\pm$  carrollite)  $\rightarrow$  bornite ( $\pm$  carrollite)  $\rightarrow$  chalcocite. This paragenetic sequence matches those reported by El Desouky *et al.* (2010), as well as some of the textural observations made by Cailteux *et al.* (2005) and Rosenfels & von der Heyden (2022).

The preceding paragraphs have considered the effects of individual physicochemical changes within the ore-forming environment, though necessarily modeling in a restricted chemical space and under the assumption that equilibrium conditions were reached. In reality, the ore-forming processes likely occur via disequilibrium processes, including biologically mediated processes, as indicated by sulfur isotope measurements (El Desouky et al. 2010). Furthermore, it is probable that the evolution of the ore fluid and the reasons for ore mineral precipitation cannot be explained by a single process. Rather, a combination of the factors described above may be needed to explain the siting, multi-scale zonation, and textural features of any given ore body. Indeed, the combination of factors and the relative importance of each factor will likely vary as a function of spatial distribution within the greater Katanga basin and as a function of which of the lithologies within the stratigraphy are mineralized. Our modeling work considers the Co and Cu solubility and the stability of Co-Cu-Fe sulfide and oxide minerals and suggests that the first order control on mineralization is the physicochemical conditions of the ore fluid. We suggest the fluid responsible for mineralizing the stratiform carrollite in the Fungurume 88 deposit was a metal-laden fluid comprising Cu and Co concentrations at or near to their respective solubility limits. An absence of co-occurring linnaeite suggests that this fluid was cooler than 211 °C (SI 5). For an assumed T of 150 °C, constraints placed by the stability field of carrollite and the overgrowths of both chalcopyrite and bornite (Fig. 3) and their respective stability limits (Fig. 8) suggest that these processes could have occurred in a broad range of oxygen fugacity and pH. Although interaction with a reducing fine-grained lithology is an efficient way to precipitate this stratiform carrollite (e.g., Rosenfels & von der Heyden 2022), trace element signatures and further modeling work suggest that changes in the T, pH, and importantly, the availability of sulfur may also have played a role.

## Conclusions

Our detailed mineralogical, mineral chemistry, and thermodynamic studies of stratiform carrollite from the Fungurume 88 deposit reveal a number of insights related both to this important battery mineral and to the genesis of the host ore body. Firstly, the dearth of published carrollite trace element data highlights that this thiospinel is somewhat understudied, a situation which is likely to change as the demand for batteries in electric vehicles continues to rise (Li & Lu 2020). From an economic perspective, and although limited to samples from a single deposit, our LA-ICP-MS data suggest that carrollite holds limited potential to host significant concentrations of 'sweetener' elements within its mineral structure. The major substituent ions identified include Fe, Ni, and excess Co that likely replaces Cu in the tetrahedral sites (Vaughan et al. 1971). Each of these elements may enter the thiospinel structure in either their divalent or trivalent state (Vaughan et al. 1971, Vaughan & Craig 1985, Wagner & Cook 1999). As such, detailed X-ray absorption spectroscopy or Mossbauer spectroscopy of this mineral may hold potential toward developing an additional redox proxy or constraint for mineralization in the CACB (i.e., as has been achieved previously by measuring Eu valence in the ore mineral scheelite; Brugger et al. 2008). As with other sulfides (e.g., Babedi et al. 2022), trace element signatures hold vast potential to reveal insights into the evolution of a hydrothermal mineralizing system. However, further work needs to be conducted on the uptake and incorporation systematics of trace elements in carrollite in order to unlock this potential.

The thermodynamic data (Gibson *et al.* 2023) and models presented herein (Figs. 5, 7, 8; SI 1, 2) represent important tools toward better understanding Co-Cu mineralization in the CACB and elsewhere globally. Coupled with the trace element fingerprints, the models suggest that a decrease in the sulfur activity within the ore-forming micro-environment may have been an important process during ore genesis. The modeling results further suggest that distinct zonation between Cu and Co endowments is favored under conditions where the

solubility contours of these two elements are markedly offset from one another. Moreover, the models suggest that a simple drop in Eh of the system is insufficient to explain reported ore textures and their associated paragenetic sequences [i.e., carrollite  $\rightarrow$  linnaeite  $\rightarrow$  Co-pentlandite (Annels & Simmonds 1984); and chalcopyrite  $\rightarrow$ bornite  $\rightarrow$  chalcocite (e.g., El Desouky et al. 2010)]. These zonation trends are better explained by increases in the pH, decreases in the T, decreases in the sulfur activity, or a combination of these factors within the ore mineralizing system.

Finally, we acknowledge that mineralization may emanate from a variety of processes [e.g., wall-rock interaction (Cailteux et al. 2005), biological mediation (El Desouky et al. 2010), fluid mixing (Sutton & Maynard 2005), anhydrite replacement (Muchez et al. 2008), etc.] and in a variety of geological settings within the  $\sim$ 400 km-long Lufillian arc. Across these various settings, the commonality is the importance of the uniqueness and anomalous metal enrichment of the ore fluid (e.g., Davey et al. 2021), which thus represents the primary factor ensuring prospectivity across the broad CACB. We posit that our presented thermodynamic models (the first to incorporate data for the major Co ore mineral carrollite) will be useful toward interrogating the nuanced controls on precipitation of ore minerals at the deposit scale from such a metal-laden ore fluid.

## ACKNOWLEDGMENTS

This work was supported by the South African DSI-NRF Centre of Excellence for Integrated Mineral and Energy Resource Analysis (CIMERA) and by the Timothy Nutt Fund from the Society of Economic Geologist (SEG). This study is based on calorimetric data generated with financial support from the U.S. Department of Energy under grant DE FG02 97ER14749. The authors would like to thank S. Lavoie and the TFM exploration team for access to the samples, and staff at the Central Analytical Facility (M. Frazenberg; A. Botes, R. Rossouw) for their assistance during the sample analyses. Finally, the authors would like to acknowledge two anonymous reviewers and Editor S. Prevec for their careful and thoughtful contributions to the final version of this manuscript.

## REFERENCES

Annels, A. & Simmonds, J.R. (1984) Cobalt in the Zambian Copperbelt. Precambrian Research 25, 75–98. DOI: https://doi.org/10.1016/0301-9268(84)90025-1

ANNELS, A.E., VAUGHAN, D.J., & CRAIG, J.R. (1983) Conditions of ore mineral formation in certain Zambian Copperbelt deposits with special reference to the role of cobalt. *Mineralium Deposita* 18, 71–88.

- Auclair, G., Fouquet, Y., & Bohn, M. (1987) Distribution of selenium in high-temperature hydrothermal sulfide deposits at 13 degrees North, East Pacific Rise. *The Canadian Mineralogist* **25**(4), 577–587.
- BABEDI, L., VON DER HEYDEN, B.P., TADIE, M., & MAYNE, M. (2022) Trace elements in pyrite from five different gold ore deposit classes: A review and meta-analysis. *Geologi*cal Society, London, Special Publications 516(1), 47–83.
- BARTON, I.F., YANG, H., & BARTON, M.D. (2014) The mineralogy, geochemistry, and metallurgy of cobalt in the rhombohedral carbonates. *The Canadian Mineralogist* 52, 653–670. DOI: https://doi.org/10.3749/canmin.1400006
- BECKETT-BROWN, C.E., McDonald, A.M., & Zhe, W. (2018) A crystallographically oriented intergrowth of siegenite (CoNi<sub>2</sub>S<sub>4</sub>) and millerite from the Morokweng impact structure, South Africa: Chemistry, texture, and origin. The Canadian Mineralogist 56, 705–722. DOI: https://doi.org/10.3749/canmin.1800007
- BENNETT, W.W. & CANFIELD, D.E. (2020) Redox-sensitive trace metals as paleoredox proxies: A review and analysis of data from modern sediments. *Earth-Science Reviews* 204, 103175.
- BEZVERKHYY, I., DANOT, M., & AFANASIEV, P. (2003) New lowtemperature preparations of some simple and mixed Co and Ni dispersed sulfides and their chemical behavior in reducing atmosphere. *Inorganic Chemistry* 42(5), 1764–1768.
- Bosi, F., Biagioni, C., & Pasero, M. (2019) Nomenclature and classification of the spinel supergroup. *European Journal* of *Mineralogy* 31(1), 183–192. DOI: https://doi.org/10. 1127/ejm/2019/0031-2788
- BRUGGER, J., ETSCHMANN, B., POWNCEBY, M., LIU, W., GRUNDLER, P., & BREWE, D. (2008) Oxidation state of europium in scheelite: Tracking fluid—rock interaction in gold deposits. *Chemical Geology* 257(1–2), 26–33.
- CAILTEUX, J., KAMPUNZU, A.B., LEROUGE, C., KAPUTO, A., & MILESI, J. (2005) Genesis of sediment-hosted stratiform copper-cobalt deposits, central African Copperbelt. *Journal of African Earth Science* 42(1–5), 134–158. DOI: https://doi.org/10.1016/j.jafrearsci.2005.08.001
- CHOUINARD, A., PAQUETTE, J., & WILLIAMS-JONES, A.E. (2005) Crystallographic controls on trace-element incorporation in auriferous pyrite from the Pascua epithermal highsulfidation deposit, Chile–Argentina. *The Canadian Min*eralogist 43(3), 951–963.
- CRAIG, J.R. & CARPENTER, A.B. (1977) Fletcherite, Cu(Ni,Co)<sub>2</sub>S<sub>4</sub>, a new thiospinel from the Viburnum Trend (New Lead Belt), Missouri. *Economic Geology* 72, 480–486.
- CRAIG, J.R., VAUGHAN, D.J., & HIGGINS, J.B. (1979) Phase relations in the Cu–Co–S system and mineral associations of the carrollite (CuCo<sub>2</sub>S<sub>4</sub>) – linnaeite (Co<sub>3</sub>S<sub>4</sub>) series. *Economic Geology* 74, 657–671. DOI: https://doi.org/10. 2113/gsecongeo.74.3.657

- DAVEY, J., ROBERTS, S., & WILKINSON, J.J. (2021) Copperand cobalt-rich, ultrapotassic bittern brines responsible for the formation of the Nkana-Mindola deposits, Zambian Copperbelt. *Geology* 49(3), 341–345.
- DEWAELE, S., MUCHEZ, P., VETS, J., FERNANDEZ-ALONZO, M., & TACK, L. (2006) Multiphase origin of the Cu-Co ore deposits in the western part of the Lufilian fold-and-thrust belt, Katanga (Democratic Republic of Congo). *Journal of African Earth Sciences* 46, 455–469. DOI: https://doi.org/10.1016/j.jafrearsci.2006.08.002
- DICK, J.M. (2019) CHNOSZ: Thermodynamic calculations and diagrams for geochemistry. Frontiers in Earth Science 7, 180. DOI: https://doi.org/10.3389/feart.2019.00180
- Dick, J.M. (2021) Diagrams with multiple metals in CHNOSZ. Applied Computing and Geosciences 10, 100059.
- EL DESOUKY, H.A., MUCHEZ, P., & CAILTEUX, J. (2009) Two Cu-Co sulfide phases and contrasting fluid systems in the Katanga Copperbelt, Democratic Republic of Congo. *Ore Geology Reviews* **36**, 315–332. DOI: https://doi.org/10.1016/j.oregeorev.2009.07.003
- EL DESOUKY, H.A., MUCHEZ, P., BOYCE, A.J., SCHNEIDER, J., CAILTEUX, J., DEWAELE, S., & VON QUADT, A. (2010) Genesis of sediment-hosted stratiform copper-cobalt mineralization at Luiswishi and Kamoto, Katanga Copperbelt (Democratic Republic of Congo). *Mineralium Deposita* 45, 735–763. DOI: https://doi.org/10.1007/s00126-010-0298-3
- FITZPATRICK, A.J. (2008) The Measurement of the Se/S Ratios in Sulphide Minerals and their Application to Ore Deposit Studies. Ph.D. thesis, Queens University, Canada. 203 pp.
- François, A. (1974) Stratigraphie, tectonique et mineralisations dans l'arc cuprifère du Shaba (Republique Du Zaire). Centenaire de la societe geologique de belgique, 79–101 (in French).
- GEORGE, L.L., COOK, N.J., CROWE, B.B.P., & CIOBANU, C.L. (2018) Trace elements in hydrothermal chalcopyrite. *Mineralogical Magazine* 82, 59–88. DOI: https://doi.org/10.1180/minmag.2017.081.021
- GIBSON, A., LILOVA, K., SUBRAMANI, T., VON DER HEYDEN, B., GILBERT, D.A., NAVROTSKY, A., & WOODFIELD, B.F. (2023) Thermodynamic properties and superconductivity of natural carrollite (CuCo<sub>2</sub>S<sub>4</sub>). The Journal of Chemical Thermodynamics, 107096.
- GREYLING, L.N. (2009) Fluid Evolution and Characterisation of Mineralising Solutions in the Central African Copperbelt. Unpublished Ph.D. thesis. University of the Witwatersrand, Johannesburg, South Africa, 266 pp. + appendices.
- GRGURIC, B.A. (2002) Hypogene violarite of exsolution origin from Mount Keith, Western Australia: Field evidence for a stable pentlandite–violarite tie line. *Mineralogical Magazine* 66, 313–326. DOI: https://doi.org/10.1180/0026461 026620032

- HELGESON, H.C., DELANY, J.M., NESBITT, H.W., & BIRD, D.K. (1978) Summary and critique of the thermodynamic properties of rock-forming minerals. *American Journal of Science* 278A, 1–229.
- HITZMAN, M., SELLEY, D., & BULL, S. (2010) Formation of sedimentary rock-hosted stratiform copper deposits through earth history. *Economic Geology* 105, 627–639. DOI: https://doi.org/10.2113/gsecongeo.105.3.627
- HITZMAN, M., BROUGHTON, D., SELLEY, D., WOODHEAD, J., WOOD, D., & BULL, S. (2012) The Central African Copperbelt: Diverse stratigraphic, structural and temporal settings in the world's largest sedimentary copper district. Society of Economic Geologists, Special Publication 16, 487–514.
- Huang, H.H. (2016) The Eh-pH diagram and its advances. *Metals* **6**(1), p.23.
- Huston, D.L., Sie, S.H., Suter, G.F., Cooke, D.R., & Both, R.A. (1995) Trace elements in sulfide minerals from eastern Australian volcanic-hosted massive sulfide deposits; Part I, Proton microprobe analyses of pyrite, chalcopyrite, and sphalerite, and Part II, Selenium levels in pyrite; comparison with delta 34 S values and implications for the source of sulfur in volcanogenic hydrothermal systems. *Economic Geology* 90(5), 1167–1196.
- IMAI, N., MARIKO, T., & SHIGA, Y. (1973) Siegenite from the Nippo ore deposit of the Kamaishi mine, Iwate Prefecture, Japan. *Mining Geology* 24, 347–354.
- JANSSON, N.F. & LIU, W. (2020) Controls on cobalt and nickel distribution in hydrothermal sulphide deposits in Bergslagen, Sweden-constraints from solubility modelling. *GFF* 142(2), 87–95.
- JEAN, G.E. & BANCROFT, G.M. (1986) Heavy metal adsorption by sulphide mineral surfaces. *Geochimica et Cosmochi*mica Acta 50(7), 1455–1463.
- KAMPUNZU, A.B. & CAILTEUX, J. (1999) Tectonic evolution of the Lufilian Arc (Central Africa Copper Belt) during Neoproterozoic Pan African orogenesis. *Gondwana Research* 2(3), 401–421.
- KEITH, M., SMITH, D.J., JENKIN, G.R., HOLWELL, D.A., & DYE, M.D. (2018) A review of Te and Se systematics in hydrothermal pyrite from precious metal deposits: Insights into ore-forming processes. *Ore Geology Reviews* 96, 269–282.
- Layton-Matthews, D., Scott, S.D., Peter, J.M., & Leybourne, M.I. (2005) Transport and deposition of selenium in felsic volcanic-hosted massive sulfide deposits of the Finlayson Lake District, Yukon Territory, Canada. *In* Mineral Deposit Research: Meeting the Global Challenge: Proceedings of the Eighth Biennial SGA Meeting Beijing, China, 18–21 August 2005, Springer Berlin Heidelberg, 643–646.
- Layton-Matthews, D., Peter, J.M., Scott, S.D., & Leybourne, M.I. (2008) Distribution, mineralogy, and geochemistry of

- selenium in felsic volcanic-hosted massive sulfide deposits of the Finlayson Lake district, Yukon Territory, Canada. *Economic Geology* **103**(1), 61–88.
- Li, M. & Lu, J. (2020) Cobalt in lithium-ion batteries. *Science* 367(6481), 979–980.
- McGowan, R.R., Roberts, S., & Boyce, A.J. (2006) Origin of the Nchanga copper–cobalt deposits of the Zambian Copperbelt. *Mineralium Deposita* 40, 617–638.
- MIGDISOV, A.A., ZEZIN, D., & WILLIAMS-JONES, A.E. (2011) An experimental study of Cobalt (II) complexation in Cl<sup>-</sup> and H<sub>2</sub>S-bearing hydrothermal solutions. *Geochimica et Cosmochimica Acta* 75(14), 4065–4079.
- MUCHEZ, P. & CORBELLA, M. (2012) Factors controlling the precipitation of copper and cobalt minerals in sedimenthosted ore deposits: Advances and restrictions. *Journal of Geochemical Exploration* 118, 38–46.
- Muchez, P. & Corbella, M. (2016) Reactive transport modelling of ore mineral zoning and the paragenesis of copper sulfides in sediment-hosted stratiform ore deposits, the Katanga Copperbelt (DRC). *Geologica Belgica* **19**(3–4), 219–223.
- MUCHEZ, P., VANDERHAEGHEN, P., EL DESOUKY, H., SCHNEIDER, J., BOYCE, A., DEWAELE, S., & CAILTEUX, J. (2008) Anhydrite pseudomorphs and the origin of stratiform Cu–Co ores in the Katangan Copperbelt (Democratic Republic of Congo). *Mineralium Deposita* 43, 575–589.
- Nazarewicz, T. (2016) Cobalt: A critical commodity. *Resource World Magazine: Mining* 52–53.
- OSTWALD, J. (1978) Linnaeite series minerals from the Kalgoorlie district, Western Australia. *Mineralogical Maga*zine 42, 93–98.
- PANKRATZ, L.B., MAH, A.D., & WATSON S.W. (1987) Thermodynamic properties of sulfides. *United States Department of the Interior, Bureau of Mines, Bulletin* 689.
- PATON, C., HELLSTROM, J., PAUL, B., WOODHEAD, J., & HERGT, J. (2011) Iolite: Freeware for the visualisation and processing of mass spectrometric data. *Journal of Analytical Atomic Spectrometry* 26, 2508–2518.
- PATTRICK, R.A.D., COKER, V.S., PEARCE, C.I., TELLING, N.D., & VAN DER LAAN, G. (2008) The oxidation state of copper and cobalt in carrollite, CuCo<sub>2</sub>S<sub>4</sub>. The Canadian Mineralogist 46, 1317–1322. DOI: https://doi.org/10.3749/canmin.46.5.1317
- Queffurus, M. & Barnes, S.J. (2015) A review of sulfur to selenium ratios in magmatic nickel-copper and platinum-group element deposits. *Ore Geology Reviews* **69**, 301–324.
- ROBB, L. (2020) Introduction to Ore-Forming Processes. John Wiley & Sons Ltd, West Sussex, UK.

- ROBIE, R.A. & HEMINGWAY, B.S. (1995) Thermodynamic properties of minerals and related substances at 298.15 K and 1 bar (10<sup>5</sup> Pascals) pressure and at higher temperatures. *U.S. Geological Survey Bulletin*, **2131**, 461–461.
- ROSENFELS, R.C. (2021) Characterising the Fungurume 88 Deposit in the Te1nke Fungurume Mining District: An Unusual, High Grade, Primary Cobalt Sulphide Deposit. M.Sc. thesis. Stellenbosch University, Stellenbosch, Western Cape province, South Africa.
- ROSENFELS, R.C. & VON DER HEYDEN, B.P. (2022) A critical comparison between the Fungurume 8 and 88 Cu-Co deposits, Central African Copperbelt. Ore Geology Reviews 140, 104627.
- SCHUH, W., LEVEILLE, R., FAY, I., & NORTH, R. (2012) Geology of the Tenke-Fungurume sediment-hosted strata-bound copper-cobalt district, Katanga, Democratic Republic of Congo. SEG Special Publication 16, 269–301.
- SHANNON, R.D. (1976) Revised effective ionic radii and systematic studies of interatomic distances in halides and chalcogenides. Acta Crystallgraphica A32, 751–767.
- SHI, Q., BOERIO-GOATES, J., & WOODFIELD, B.F. (2011) An improved technique for accurate heat capacity measurements on powdered samples using a commercial relaxation calorimeter. *The Journal of Chemical Thermodynamics* 43(8), 1263–1269.
- SHI, Q., SNOW, C.L., BOERIO-GOATES, J., & WOODFIELD, B.F. (2010) Accurate heat capacity measurements on powdered samples using a Quantum Design physical property measurement system. *Journal of Chemical Thermody*namics 42(9) 1107–1115.
- SHOCK, E.L. & HELGESON, H.C. (1988) Calculation of the thermodynamic and transport properties of aqueous species at high pressures and temperatures: Correlation algorithms for ionic species and equation of state predictions to 5 kb and 1000 C. Geochimica et Cosmochimica Acta 52(8), 2009–2036.
- SUBRAMANI, T., LILOVA, K., ABRAMCHUK, M., LEINENWEBER, K. D., & NAVROTSKY, A. (2020) Greigite (Fe<sub>3</sub>S<sub>4</sub>) is thermodynamically stable: Implications for its terrestrial and planetary occurrence. *Proceedings of the National Academy Science* 117, 28645–28648.
- SUTTON, S.J. & MAYNARD, J.B. (2005) A fluid mixing model for copper mineralization at Konkola North, Zambian Copperbelt. *Journal of African Earth Sciences* 42(1–5), 95–118.
- SVERJENSKY, D.A., SHOCK, E.L., & HELGESON, H.C. (1997) Prediction of the thermodynamic properties of aqueous metal complexes to 1000 C and 5 kb. Geochimica et Cosmochimica Acta 61(7), 1359–1412.

- SWEENEY, M., TURNER, P., & VAUGHAN, D.J. (1986) Stable isotope and geochemical studies in the role of early diagenesis in ore formation, Konkola Basin, Zambian copper belt. *Economic Geology* 81(8), 1838–1852.
- TWIGG, H., HITZMAN, M., & BRODBECK, M. (2022) Using LA-ICP-MS trace-element sulphide mapping to delineate multiphase Co-Cu mineralisation in the Kakanda deposits, Central African Copperbelt DRC Implications for Re-Os dating. Society of Economic Geologists biannual meeting, August 27 30, 2022, Denver, Colorado, USA.
- ULLRICH, M.K., POPE, J.G., SEWARD, T.M., WILSON, N., & PLANER-FRIEDRICH, B. (2013) Sulfur redox chemistry governs diurnal antimony and arsenic cycles at Champagne Pool, Waiotapu, New Zealand. *Journal of Volcanology* and Geothermal Research 262, 164–177.
- UNRUG, R. (1988) Mineralization controls and source of metals in the Lufilian fold belt, Shaba (Zaire), Zambia and Angola. *Economic Geology* 83(6), 1247–1258. DOI: https://doi.org/10.2113/gsecongeo.83.6.1247
- VASYUKOVA, O.V. & WILLIAMS-JONES, A.E. (2022) Constraints on the genesis of cobalt deposits: Part II. Applications to natural systems. *Economic Geology* 117(3), 529–544. DOI: https:// doi.org/10.5382/econgeo.4888
- VAUGHAN, D.J. & CRAIG, J.R. (1985) The crystal chemistry of iron-nickel thiospinels. *American Mineralogist* 70(9–10), 1036–1043.
- VAUGHAN, D.J., BURNS, R.G., & BURNS, V.M. (1971) Geochemistry and bonding of thiospinel minerals. *Geochimica Cosmochimica Acta*. 35, 365–381. DOI: https://doi. org/10.1016/0016-7037(71)90079-2
- Wagner, T. & Cook, N.J. (1999) Carrollite and related minerals of the linnaeite group: Solid solutions and nomenclature in the light of new data from the Siegerland district, Germany. *The Canadian Mineralogist* 37, 545–558.
- WILBURN, D.R. (2012) Cobalt mineral exploration and supply from 1995 through 2013. USGS Scientific Investigations Report 2011-5084.
- WILLIAMS-JONES, A.E. & VASYUKOVA, O.V. (2022) Constraints on the genesis of cobalt deposits: Part I. Theoretical considerations. *Economic Geology* 117(3), 513–528. DOI: http://doi.org/10.5382/econgeo.4895
- YAMAMOTO, M. (1976) Relationship between Se/S and sulfur isotope ratios of hydrothermal sulfide minerals. *Minera-lium Deposita* 11, 197–209.
- Received April 26, 2023. Revised manuscript accepted October 5, 2023.
- This manuscript was handled by Editor Stephen Prevec.